Sakarya University Journal of Science

ISSN : 2147-835X
Publisher : Sakarya University

Vol. 28, No. 5, 984-999, 2024
DOI: https://doi.org/10.16984/saufenbilder.1478566

Research Article

Eco-Friendly Green Synthesis of Zinc Oxide Nano/Microparticles Using Aqueous Leaf Extract of *Polygonum cognatum* Meisn. Plant

Erdem Akça

Sivas Cumhuriyet University, Department of Metallurgical and Materials Engineering, Faculty of Engineering, Sivas, Türkiye, erdemakca@cumhuriyet.edu.tr

ARTICLE INFO

Keywords:
Green synthesis
Polygonum cognatum Meisn
Zinc oxide
Powder characterization
Nanoparticles

Article History:
Received: 04.05.2024
Accepted: 06.08.2024
Online Available: 14.10.2024

ABSTRACT

The environmentally friendly plant-based green synthesis approach provides a fabulous opportunity to produce versatile zinc oxide powders with multifarious morphology and/or size. In this study, it was mainly aimed at using *Polygonum cognatum* Meisn. extract to synthesize zinc oxide powder via a simple green synthesis route. For this purpose, zinc nitrate solution was mixed with an aqueous extract of fresh *Polygonum cognatum* Meisn. plant leaves to obtain a zinc-based precursor, and then zinc oxide powder was synthesized by means of calcination conducted at 400°C for 2 hours in air. Phase, spectroscopic, and microstructural analysis techniques, as well as Rietveld refinement method and Williamson-Hall analysis, were performed to investigate the powder characteristics. It was found that the synthesized high-purity zinc oxide powder had a hexagonal wurtzite crystal structure. Zinc oxide powder was observed to have a particularly large amount of nano-sized equiaxed particles (~25 nm in average diameter) together with micron-sized hourglass-like particles consisting of two hexagonal prisms (each <1 μm in height). All in all, the main implication of our research is that the *Polygonum cognatum* Meisn. plant can be potentially used as a biomass source for the green synthesis of zinc oxide nano/microparticles.

1. Introduction

Zinc oxide (ZnO) is an important inorganic material with multifunctional characteristics due to its unusual physical, chemical, or biological properties [1–3]. Therefore, it is unsurprising that ZnO attracts great attention in technological areas and scientific studies. In the global market, ZnO-based products are mainly demanded by various industries, ranging from rubber, ceramic, and paint manufacturing to agricultural, food, pharmaceutical, electronics [4–6]. It stands out that the scientific community has made tremendous efforts to improve the properties and performance of zinc oxide-based compounds, particularly in powdery forms. Nano- and micrometer-sized zinc oxide particles have been synthesized through chemical, physical, and biological processing approaches [4, 6–8].

Green synthesis routes, one of the most creative bottom-up synthesis methods, distinguish themselves from the others due to their straightforward implementation, cost-effectiveness, eco-friendliness, and safety characteristics. The green synthesis procedure is considered a cleaner, more reliable, and more sustainable technique since it mainly requires biomass resources, non-toxic solvents and results in negligible waste and pollutant formation [2, 6, 9–11].

Biogenic compounds are usually derived from the most abundant life forms, i.e., plants, bacteria, algae, fungi, etc., by simple extraction methods. Especially, plant-based phytochemicals with chemical functional groups are widely used for reducing, stabilizing, and/or capping agents for metallic ions in the solvents. There are innumerable scientific studies in the

Cite as: E. Akça (2024). Eco-Friendly Green Synthesis of Zinc Oxide Nano/Microparticles using Aqueous Leaf Extract of Polygonum cognatum Meisn. Plant, *Sakarya University Journal of Science*, 28(5), 984-999. https://doi.org/10.16984/saufenbilder.1478566

literature related to laboratory-scale processing, characterizations, and applications of the green synthesis of zinc oxide particles [11–27].

Polygonum cognatum Meisn., colloquially known as "Madımak", belongs to the Polygonaceae family, which is a perennial plant that grows naturally in various regions of Anatolia in Türkiye at altitudes ranging from 720 to 3000 meters. The shoots and leaves of this plant are usually consumed as meals in Central Anatolian cuisine, as well as used for some traditional medicinal purposes [28–37]. *Polygonum cognatum* Meisn. contains phytochemical compounds, i.e., phenolics, vitamins, flavonoids, and carotenoids together with some macro- and micro-nutrients [28, 29, 31–38]. Moreover, previous studies have shown the presence of antioxidant, antimicrobial, cytotoxic, or antiproliferative activities in extracts derived from this plant [28, 31, 35, 36, 38–40]. Recently, many scientists have shown great interest in the *Polygonum cognatum* spices for research and development activities in the fields of medicine, pharmacy, agriculture, biology, chemistry, biochemistry, etc.

Polygonum cognatum plant extract possesses potential phytochemicals that can be used for green synthesis; however, there are few papers related to the biosynthesis of nano-sized particles using *Polygonum cognatum* plant extract in the literature. It was reported that metallic nanoparticles of copper, iron, or silver (ranging from 20 to 100 nm) were synthesized through extracts derived from *Polygonum cognatum* plant [41–43]. In addition, magnetite-reduced graphene oxide particles prepared using the aqueous extract of *Polygonum cognatum* as a stabilizing and reducing agent [44]. To the best of our knowledge, there is a gap in the literature about the green synthesis of metal oxide particles by using *Polygonum cognatum* spices. We believe that the *Polygonum cognatum* Meisn. plant could be a promising natural resource for green chemistry processing of metal oxide particles due to its bioactive components.

The main motivation of this study is to demonstrate the green synthesis of ZnO particles by using the *Polygonum cognatum* Meisn. plant. For this purpose, the aqueous extract was first obtained from the fresh leaves of the *Polygonum cognatum* Meisn. plant collected in Sivas Province, Türkiye. Next, the reaction between zinc nitrate hexahydrate and plant extract solutions yielded the precursor. Finally, zinc oxide was synthesized via solid-state calcination of the precursor, and XRD, SEM/EDS, STEM analyses, as well as spectroscopic characterizations (FT-IR, UV-Vis, and Raman spectroscopy) were carried out.

2. Materials and Methods

Zinc nitrate hexahydrate ($Zn(NO_3)_2 \cdot 6H_2O$) (≥98%, Tekkim) was the sole chemical raw material as a zinc source used as received without further purification in this study. Figure 1 shows the steps of the green synthesis for zinc oxide in detail.

In the first step, fresh *Polygonum cognatum* Meisn. plant collected in rural areas of Sivas Province (Türkiye) was purchased from the domestic market hall located in the downtown. The plant was kept in tap water in the deep, transparent container for a while. Thereby, it was easy to remove dirt and unwanted foreign substances since those had sunk to the bottom. Following that, we repeatedly washed the plant leaves, which had separated from the stem, in distilled water.

In the second step, 40 grams of fresh leaves were soaked in 400 ml of distilled water in a 600 ml beaker and mixed for 2 hours on a hot plate at 75°C with continuous stirring. The beaker was covered by PVC cling film to minimize evaporation during the process. Also, the constant temperature was maintained by using an external thermocouple attached to the magnetic stirrer. The mixture, which turned into a brownish-green color, was left for a while in the laboratory to cool down naturally to room temperature. The extract solution was filtered through Whatman filter paper (No. 1) and centrifuged at 15,000 rpm for 3 min. Subsequently, it was stored in the refrigerator until the next use.

Figure 1. Detailed processing steps for the green synthesis of zinc oxide particles

In the third step, 50 ml of the extract solution poured into a 250 ml beaker on a hot plate was heated up with continuous stirring at 400 rpm until temperature reached 60°C. Then, 50 ml of 1 M zinc nitrate hexahydrate solution was gradually dripped into the heated extract solution. During this process, the formation of suspended gel-like small particles in the mixture, which was probably due to the reaction between zinc ions and bioactive compounds, could be immediately observed. The mixture with 50:50 (% v/v) in a covered beaker was stirred at 300 rpm at 60°C for 3 h.

Subsequently, the temperature of the hot plate was increased above 100°C to evaporate the excess water in the heated mixture. Also, a fan was placed on the beaker after removing the PVC cling film. Meanwhile, the mixture turned into a viscous fluid with a brownish-orange color during the 7-hour heating procedure. 75 ml of distilled water was poured into the viscous fluid and then sonicated for 15 min. It was transferred into the polypropylene measuring cylinder to ensure the spontaneous sinking of the precipitate to the bottom. The supernatant was removed for each step before refreshing the water. Thereby, the precipitate was rinsed with distilled water several times to remove any unwanted excess. Eventually, dried participate was put in the porcelain crucible and calcined at 400°C for 2 h with 5°C/min heating and cooling rates in air.

The phase formation of the powder was checked by an X-ray diffractometer (XRD) (Rigaku Miniflex600, Japan) using Cu*K*α radiation. Rietveld refinement for the XRD data of ZnO powder was carried out using MAUD software (Materials Analysis Using Diffraction, Version 2.9993) [45]. Microstrain (ε) and crystallite size (*D*) were determined by using Williamson-Hall analysis [46]. The microstructure and elemental analysis of powder were examined by a field emission scanning electron microscopy (SEM) equipped with an energy dispersive spectroscopy (EDS) detector and a STEM detector (TESCAN MIRA3 XMU). Attenuated total reflection Fourier-transform infrared (ATR-FTIR) spectrum was recorded in the range of 4000–400 cm^{-1} (Bruker, Tensor II). A UV–Vis diffuse reflectance spectroscopy (Thermo Scientific Evolution 201) was used to determine the band gap of ZnO in the wavelength range of 200–800 nm. The Raman spectrum of calcined powder was measured directly by using Raman spectroscopy with a 532 nm laser (Jasco NRS4500 confocal Raman microspectroscopy) performed between 95 and 875 cm^{-1}.

3. Results and Discussion

Figure 2 shows the X-ray diffraction patterns of green synthesized powder zinc oxide calcined at 400°C for 2 h. The peaks observed at 2θ = 31.76° (100), 34.42° (002), 36.26° (101), 47.54° (102), 56.58° (110), 62.84° (103), 66.36° (200), 67.97° (112), 69.08° (201), 72.58° (004), and 76.92°

(202) nicely correspond to the characteristic peaks of zincite crystal (JCPDS card # 36-1451). In addition, Rietveld analysis was performed to determine the crystal structure of synthesized ZnO particles based on the Crystallographic Information File (CIF) of the zincite mineral (card no. 2300450) obtained from Crystallography Open Database [47]. During the refinement process, all indexed peaks were used, excluding the *K*β peak (at 2θ~28°) arose from the instrumental setup. The experimental diffraction data (Y_{obs}), the calculated diffraction data (Y_{cal}), and their difference (Y_{obs}-Y_{cal}) were demonstrated in Figure 2, as well as the peak positions of zincite (vertical blue lines).

The Rietveld refinement output of R_b (%) = 6.83, R_{wp} (%) = 7.65, R_{exp} (%) = 3.41, and χ^2 = 2.24 obviously indicated that the calculated data was in good agreement with the observed ones. In other words, the XRD pattern revealed that the peaks match well with the zincite ZnO. Besides, the lattice parameters such as unit cell lengths, angles, and volume for synthesized particles were computed as a=b= 3.2508 Å ±7.59E-5, c= 5.2074 Å ±1.37E-4 (c/a= 1.60188), α=β= 90°, γ= 120°, and V= 47.656 Å^3. It means that the green synthesized zinc oxide particles clearly possess a hexagonal wurtzite-type crystalline structure.

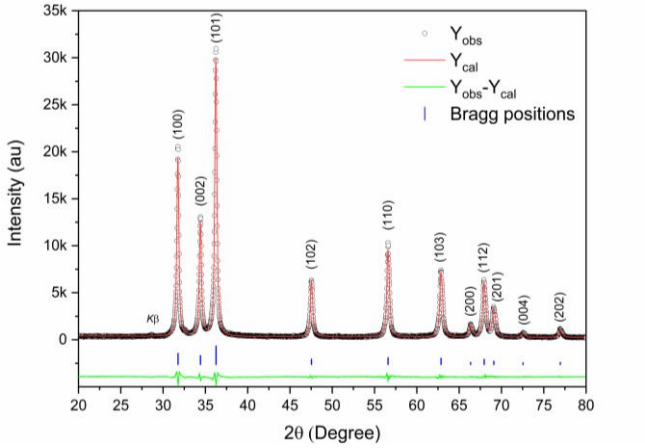

Figure 2. X-ray diffraction patterns of green synthesized calcined zinc oxide powder and Rietveld refinement result

Meanwhile, bond length (*L*) between Zn and O was calculated as 1.9783 Å by using lattice parameters based on the equation (1) [48].

$$L = \sqrt{\left(\frac{a^2}{3} + c^2\left(\frac{1-2u}{2}\right)^2\right)} \quad (1)$$

where both *a* and *c* are unit cell lengths, *u* is the positional parameter ($u = \left[1/4 + 1/3\,(a/c)^2\right]$). On the other hand, Williamson-Hall analysis was carried out based on the equation (2) to determine the lattice strain and crystallite size of green synthesized zinc oxide powder [46].

$$\beta_{hkl}cos\theta = \frac{K\lambda}{D} + 4\varepsilon sin\theta \quad (2)$$

where β_{hkl} is the peak broadening, *K* is the shape factor (0.94), λ is the wavelength of Cu*K*α radiation (1.5406 Å), *D* is crystallite size, and ε is the lattice microstrain. β_{hkl} values were obtained from the full width of half maximum (FWHM) of each XRD peak estimated by using the Voigt model. Figure 3 depicts the Williamson-Hall plot together with linear regression results for green synthesized zinc oxide powder. The crystallite size (*D*) and microstrain (ε) values, which are obtained by the intercept on the *y*-axis and the slope of linear fit line, respectively, are 48 nm and 0.00133 for calcined zinc oxide powder.

Powder characteristics could differ based on the processing conditions, raw materials, ingredients, etc. For example, the crystallite size and microstrain values for ZnO powders synthesized via similar green routes by using various plant-based extracts and calcined at 400°C were reported to be D = 4.5-17.8 nm and ε = 0.0065-0.0078 in a previous work [49], whereas another study reported $D \approx 35$ nm and ε = 0.000346 [50].

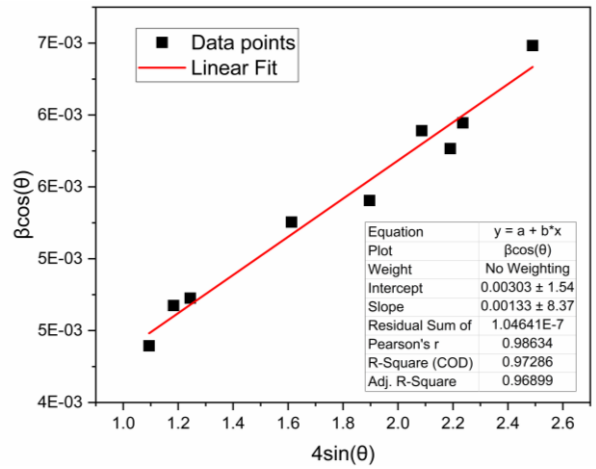

Figure 3. Williamson-Hall plot of green synthesized zinc oxide powder

FTIR spectroscopy is a practical tool for analyzing the functional groups of materials. Figure 4 depicts the room-temperature ATR-FTIR spectrum of the green synthesized ZnO particles taken in the range between 400 and 4000 cm^{-1}. All prominent absorption peaks at 479, 552, 705, 1055, 1396, 1624, 2097, 2343, and 3382 cm^{-1} were marked in the FTIR spectrum. The absorption peaks observed at 479, 552, and 705 cm^{-1} highly likely belong to zinc oxide with a hexagonal wurtzite structure. The absorption bands around 400-700 cm^{-1} were reported to be

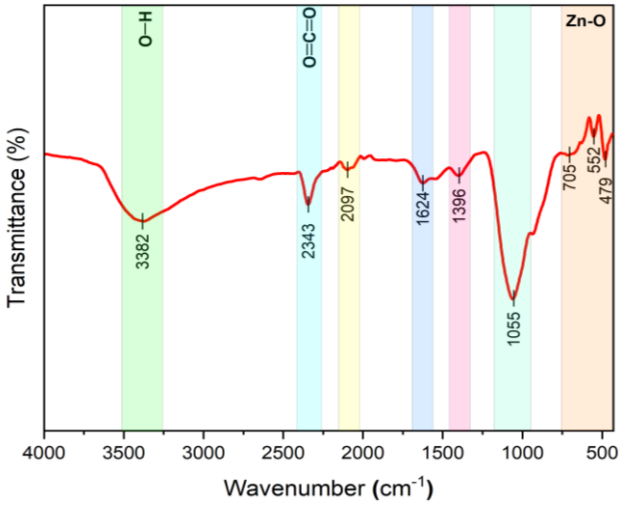

Figure 4. ATR-FTIR spectrum of green synthesized zinc oxide particles

associated with the Zn–O stretching in the zinc oxide lattice in pervious works [20, 22, 49–55]. Especially, the strong peak at 479 cm^{-1} that appeared in the FTIR spectrum was very close to the ones stated as the characteristic absorption peak for ZnO. On the other hand, the explicit peaks at ~2343 and 3382 cm^{-1} were undoubtedly corresponding to the characteristic O-H stretching and O=C=O stretching arising from atmospheric moisture and carbon dioxide, respectively [14, 20, 55]. In addition, there were some divergent evaluations about the other absorption bands between ~1000 and 3000 cm^{-1} could belong to various functional groups of organic compounds with stretching or bending vibrations, i.e. C=C, C=O, C−N, C−H, etc [14, 20, 49, 51, 53]. Meanwhile, it was also possible that some residual matters, resulting from organic extracts used for the green synthesis of zinc oxide, remained in the structure due to the low heat treatment procedure [20, 22, 50, 55].

Raman spectroscopy is one of the most useful characterization techniques that provides insight into the chemical fingerprints of various materials. Figure 5 shows the room-temperature Raman spectrum of the green synthesized ZnO particles taken in the spectral range between 95 and 875 cm^{-1}. All distinguishable peaks at 100, 118, 165, 263, 334, 380, 410, 438, 579, 685, and

812 cm^{-1} were marked in the Raman spectrum. The optical phonons (Γ_{opt}) at the center of the Brillouin zone can be described as $\Gamma_{opt} = A_1 + E_1 + 2E_2 + 2B_1$ for the crystalline zinc oxide with a hexagonal wurtzite structure, which is a member of the $P6_3mc$ space group. The Raman active polar modes of A_1 and E_1 split into the vibration modes of transvere optical (*TO*) and longitudinal

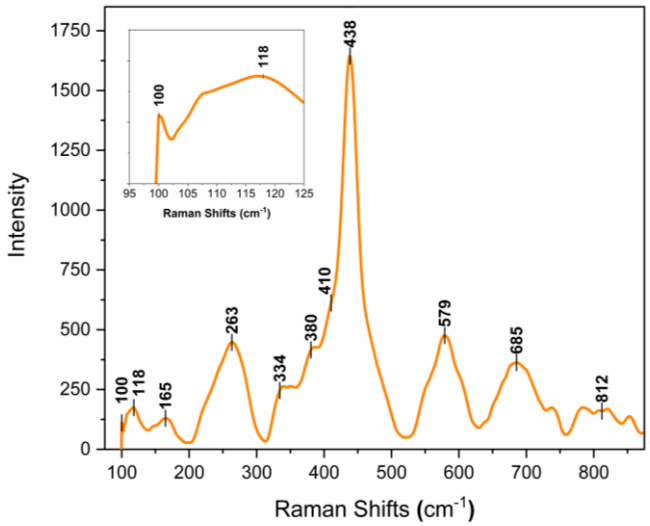

Figure 5. Room-temperature Raman spectrum of green synthesized zinc oxide particles

optical (*LO*), whereas E_2 modes (E_2^{low} and E_2^{high}) are Raman active but exhibiting a non-polar nature. On the other hand, the B_1 modes are silent, in other words, Raman inactive [56]. The peaks at 100 cm^{-1} and 438 cm^{-1} are the characteristic phonon modes belonging to ZnO, designated as E_2^{low} and E_2^{high}, respectively [56, 57]. The vibration of zinc atoms results in low-frequency phonon mode (E_2^{low}), whereas high-frequency phonon mode (E_2^{high}) is associated with the vibration of oxygen atoms. On the other hand, the sharp intense peak observed at 438 cm^{-1} is an obvious indication of the hexagonal wurtzite structure of zinc oxide [58–60].

Meanwhile, the peaks at 118 cm^{-1} and 165 cm^{-1} could arise from E_2^{low} asymmetric tail ($E_2^{low, tail}$) modes [57]. The peaks located at 334 cm^{-1} and 410 cm^{-1} are related to the E_2^{high}–E_2^{low} and $E_1(TO)$, respectively [56]. As for the Raman active polar of A_1, the peaks at 380 cm^{-1} and 579 cm^{-1} highly likely correspond to A_1 (*TO*) and A_1 (*LO*) modes, respectively [56, 57]. The peaks at 263 and 812 cm^{-1} could be associated with the B_1 silent modes. Those modes were reported as B_1^{low} at 261 cm^{-1} and B_1^{low}+B_1^{high} at 810 cm^{-1} [61], which were predicted by the calculations for wurtzite-type zinc oxide in earlier works. The silent peaks seen in the Raman spectrum of zinc oxide could be activated due to the lattice disorder or defects triggered by impurities, dopants, secondary phases, or processing conditions [56, 58, 61].

The activation of the Raman inactive B_1 silent modes was believed to be linked to probable minor amounts of elements resulting from raw materials and/or plant extract used for green synthesized zinc oxide. On the one hand, we assumed that the peak at 685 cm^{-1} was a combination of several peaks nearby. According to peak-fit analysis (not shown here), there were highly likely two separated multiphonon peaks at 674 and 700 cm^{-1}, which was in good agreement with the literature results [56, 57].

Figure 6 shows the UV-Vis spectrum of synthesized zinc oxide powder in the range between 200 and 800 nm, together with the Tauc plot. There is an obvious absorption peak appeared at 375 nm, which is within the UVA region, in the UV-Vis spectrum of the powder. The absorption peak values were reported to be typically between 367 and 393 nm for various zinc oxide powders synthesized by means of the plant-based green chemistry route [14, 27, 49, 50, 53].

The absorption peak at 375 nm was close to the characteristic peak for ZnO with a hexagonal wurtzite crystal structure. In some cases, a red-shift or blue-shift of the absorption peak for ZnO

in the UV-Vis spectrum could be observed due to the processing parameters (i.e., impurities, doping, concentration, calcination temperature, etc.) [14, 49, 50]. The Tauc plot (see inset in Figure 6.) was used to ascertain the optical band gap energy (E_g) of synthesized zinc oxide powder. The plot of energy vs $(\alpha h\nu)^2$, in other words, the Tauc plot, was obtained based on the equation (3) [62].

$$(\alpha h\nu)^{1/\gamma} = A\left(h\nu - E_g\right) \quad (3)$$

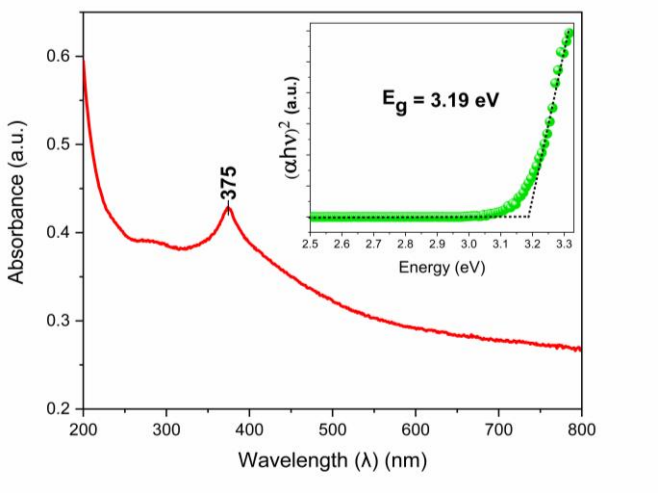

Figure 6. UV-Vis spectrum of the zinc oxide powder and the Tauc plot

where α is the energy-dependent absorption coefficient, *h* is the Planck's constant, ν is the photon's frequency, *A* is energy-independent constant, E_g is the optical band gap energy, and γ is the coefficient related to the nature of the electron transition and corresponds to 1/2 or 2 for direct and indirect allowed transition band gaps, respectively. The direct E_g was represented by the intersection of the *x*-axis of the Tauc plot, which was determined with the help of the extrapolation of linear fitting, where an abrupt increase in the values of $(\alpha h\nu)^2$. The direct E_g of synthesized zinc oxide powder was estimated at 3.19 eV. It is known that the direct E_g is approximately 3.37 eV for zincite mineral with a hexagonal wurtzite crystal structure [4, 21]. In addition, it is seen that direct bandgap values between 3 and 3.37 eV to have been reported for pure zinc oxide powder produced by various green synthesis methods in the literature [14, 20, 49, 63].

Figure 7 demonstrates the SEM micrographs and EDS analyses of calcined powder. The low-magnification image in Figure 7a represents the general view of agglomerated calcined powder. There are three distinct types of particle shapes, such as nano-sized round-like, micron-sized hourglass-like, and sub-micron plate-like shown in Figure 7b-d. Plenty of nano-sized round-like particles stand out as well as a considerable amount of micron-sized hourglass-like particles and few amounts of sub-micron plate-like particles. It is highly likely that several bioactive phytochemical compounds, especially phenolics, vitamins, flavonoids, or carotenoids in the *Polygonum cognatum* Meisn. extract, act as reducing, stabilizing, and/or capping agents for Zn^{2+} metallic ions in the solution. During the green synthesis procedure, disassociated Zn^{2+} ions from zinc nitrate solution were probably attached to functional groups of biogenic compounds in the extract due to interaction between them; therefore, the nucleation arose in the early stages of the process. Then, particle growth occurred as a result of the Ostwald ripening mechanism, and thereby a zinc-based intermediate complex precipitated [2, 9, 10, 12, 13, 21].

Besides, a calcination procedure (200-900°C, most preferably about 400°C) is usually required to transform an intermediate compound consisting of the coalescence of very small precursors into crystalline pure zinc oxide nano- or micro-particles [2, 16, 20, 50]. During the solid-state calcination step, smaller particles are basically consumed by bigger ones thanks to the Ostwald ripening mechanism. Particularly, the agglomeration tendency of nano-sized particles

with higher surface energy is supposed to have been responsible for the formation of bigger, micron-sized hexagonal columnar particles via the heat treatment process.

The exiting of small precipitates on the hexagonal columnar particles seen in Figure 7c was considered as the evidence of the aforesaid growth mechanism. Meanwhile, hexagonal prism-shaped zinc oxide particles essentially resembled hourglass-like morphology (max. ~2 µm in height). Similar micron-sized zinc oxide particles were reported to be synthesized by various methods [64–68], i.e. chemical bath deposition, hydrothermal, sol-gel, combined ultrasonic/microwave irradiation, etc. Indeed, the hourglass-like morphology consisted of two

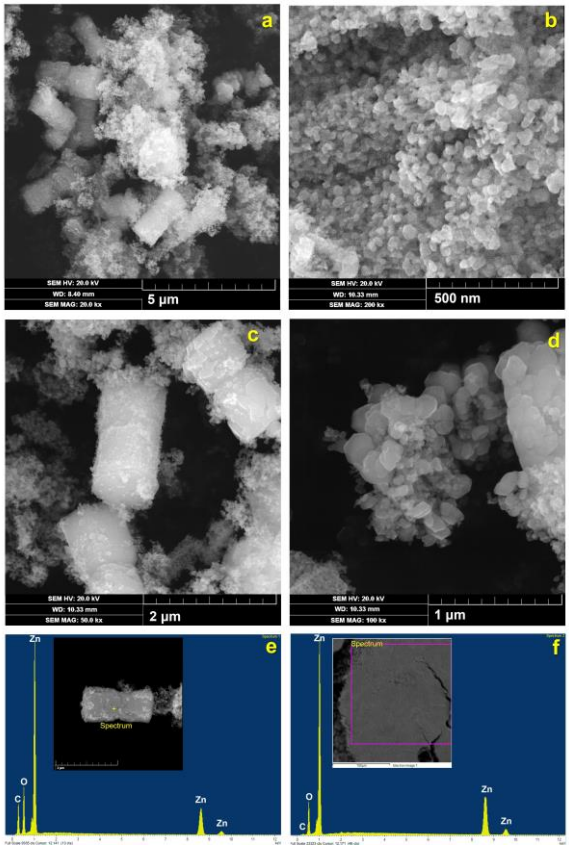

Figure 7. SEM micrographs and EDS analyses of green synthesized ZnO particles. General view of agglomerated calcined powder (a), nano-sized round-like particles (b), micron-sized hourglass-like particles (c), sub- micron plate-like particles (d), EDS spectrum of hourglass-like particle (e), and EDS spectrum of synthesized zinc oxide powder (f)

identical hexagonal prisms, that is, dimer structure.

Each ZnO microcrystal with a hexagonal prism shape typically possesses two polar planes: (0001) at the top and $(000\bar{1})$ at the down of the wurtzite unit cell. Previous studies highlighted the effects of the Ostwald ripening phenomenon, van der Waals interaction, and/or electrostatic interactions on the nucleation, the aggregation of small particles, and the formation of hexagonal dimer structures of ZnO [65, 66, 68]. It was believed similar mechanism(s) resulted in the formation of small-sized truncated hexagonal prisms with approximately 800 ±100 nm in height and 500 ±50 nm in side-length of base in the first stages of the process. It was highly likely that the final hourglass-like dimer structure emerged when two hexagonal prisms joined each other by virtue of the coupling of their (0001) planes [65, 66, 68].

EDS analysis clearly indicated that the presence of zinc and oxygen atoms for the individual hourglass-like particle shown in Figure 7e. According to the ESD analysis taken from the larger area of the suppressed powder shown in Figure 7f, atomic ratios were found to be 44.59% of Zn, 54.50% of O, 0.53% of P, 0.22% of S, and 0.13% of Cl, except for C from conductive

carbon tape. Note that characteristic peaks of negligible amounts of minor elements cannot be well distinguishable compared to the main elements (Zn and O) in the EDS spectrum in Figure 7f. Some residual elements were known to remain in the green synthesized zinc oxide by using the plant extract after even high-temperature calcination (≥ 400°C) [14, 50].

For instance, *Polygonum cognatum* Meisn. plant extract was reported to involve some elements such as P, S, Cl, N, etc. in previous works [31, 69]. Also, residual elements could be attributed to the used zinc nitrate hexahydrate raw material with ≥98% purity, which was used in this study. Regardless of the origin of residuals, the existence of minor elements was believed to be associated with their energetic stability at the calcination temperature of 400°C. This temperature was very close to the most preferred ones for synthesized zinc oxide powders in the literature. Actually, the aim of the calcination is to ensure the formation of a crystalline phase together with the decomposition and/or burnout of residual matters come from the plant extract. Maybe a higher calcination temperature is useful in terms of being free from residuals; however, the risk of the exaggerated particle growth and the deterioration of morphology should be taken into account at the same time. Given that the overall phase characteristics of green synthesized zinc oxide in our study were in good agreement with those reported in the literature, the calcination temperature of about 400°C was believed to be reasonable.

Figure 8 depicts the STEM images of nanoparticles separated from synthesized zinc oxide powder, particle size distribution, and the Tyndall effect of colloidal suspension. Figure 8a-b shows STEM images of nanoparticles isolated from synthesized zinc oxide powder by simple procedure. Briefly, a small amount of ZnO powder was added to distilled water and subjected to ultrasonic energy, then kept stationary. It was observed that the larger particles settled down immediately owing to the gravitational force, while nanoparticles suspended in the distilled water exhibited colloidal dispersion behavior. The isolated nanoparticles stand out as having a virtually equiaxed particle shape together with 24.8 nm of mean particle size, as seen in Figure 8c. In addition, the Tyndall effect was conspicuously observed for nanoparticles suspended in the distilled water that exhibited colloidal dispersion behavior because the light beam from the laser source dramatically scattered due to the strong interaction with the suspended nanoparticles (see Figure 8d). On the contrary, the light was invisible in distilled water because it directly passed through without any interaction.

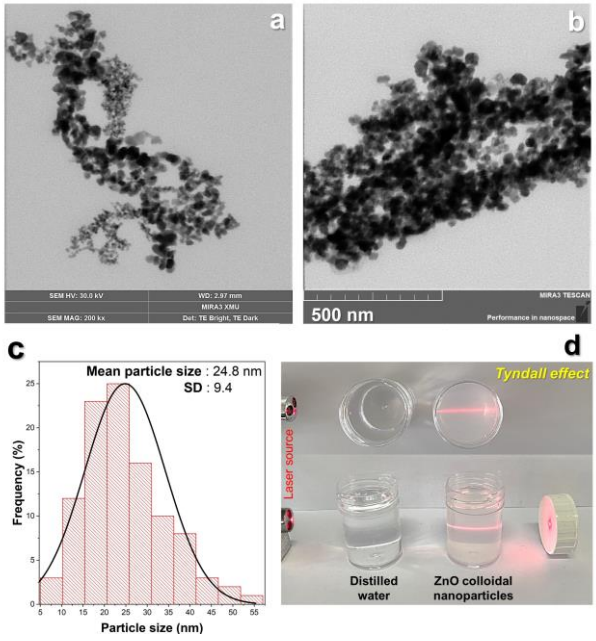

Figure 8. STEM image of nanoparticles (a-b), particle size distribution (c), the Tyndall effect of colloidal zinc oxide particles (d).

Indeed, the number, morphology, size, and purity of the particles strongly depend on the process parameters of the green synthesis procedure, especially the type of plant species and their ingredients, the concentration of the raw material and extract, the pH of the solutions, reaction time and temperature, calcination temperature, etc. In this study, we essentially focused on the specific process parameters to find out whether or not the *Polygonum cognatum* Meisn. could be a promising plant in terms of the green synthesis of zinc oxide. In the light of these results, particle characteristics, especially size and morphology, of zinc oxide particles can be tailored for various applications by using *Polygonum cognatum* Meisn. extract thanks to future systematic studies.

4. Conclusion

The aim of the current study is to reveal the potential of using *Polygonum cognatum* Meisn. plant extract in the green synthesis of zinc oxide powder. Zinc oxide powder was synthesized via the calcination at 400°C for 2 hours of the precursor, which was obtained by mixing zinc nitrate solution and *Polygonum cognatum* Meisn. aqueous leaf extract with the specific process conditions. X-ray diffraction, spectroscopic, and microstructural analysis techniques were used for the powder characterizations.

The results obviously demonstrated that the synthesized powder was pure zinc oxide with a hexagonal wurtzite crystal structure (a=b= 3.2508 Å, c= 5.2074 Å, α=β= 90°, and γ= 120°). The crystallite size and microstrain values were estimated at 48 nm and 0.00133, respectively. The direct allowed E_g was calculated as 3.19 eV based on the absorption peak observed at 375 nm in the UV-Vis spectrum of zinc oxide powder. It was found that equiaxed nanoparticles with a mean particle size of ~25 nm were accompanied by hourglass-like microparticles, which consisted of two hexagonal prisms with a height of <1 μm each. In conclusion, the main implication of this study is that the *Polygonum cognatum* Meisn. plant extract can be a promising biomass source to tailor the green synthesis of zinc oxide nano/microparticles with various morphologies, which can be used for numerous technological applications.

Article Information Form

Funding
The author has not received any financial support for the research, authorship, or publication of this study.

The Declaration of Conflict of Interest/ Common Interest
No conflict of interest or common interest has been declared by the authors.

The Declaration of Ethics Committee Approval
This study does not require ethics committee permission or any special permission.

The Declaration of Research and Publication Ethics
The authors of the paper declare that they comply with the scientific, ethical and quotation rules of SAUJS in all processes of the paper and that they do not make any falsification on the data collected. In addition, they declare that Sakarya University Journal of Science and its editorial board have no responsibility for any ethical violations that may be encountered, and that this study has not been evaluated in any academic publication environment other than Sakarya University Journal of Science.

References

[1] A. Czyżowska, A. Barbasz, "A review: zinc oxide nanoparticles – friends or enemies?," International Journal of Environmental Health, vol. 32, no. 4, pp. 885–901, 2022.

[2] S. Zeghoud, H. Hemmami, B. Ben Seghir, I. Ben Amor, I. Kouadri, A. Rebiai, M. Messaoudi, S. Ahmed, P. Pohl, J. Simal-Gandara, "A review on biogenic green synthesis of ZnO nanoparticles by plant biomass and their applications," Materials Today Communications, vol. 33, Dec. 2022, Art. no. 104747.

[3] C. B. Ong, L. Y. Ng, A. W. Mohammad, "A review of ZnO nanoparticles as solar photocatalysts: Synthesis, mechanisms and applications," Renewable and Sustainable Energy Reviews, vol. 81, pp. 536–551, Jan. 2018.

[4] A. Kołodziejczak-Radzimska, T. Jesionowski, "Zinc Oxide—from synthesis to application: A review," Materials, vol. 7, no. 4, pp. 2833–2881, Apr. 2014.

[5] P. Sharma, M. R. Hasan, N. K. Mehto, Deepak, A. Bishoyi, J. Narang, "92 years of zinc oxide: has been studied by the scientific community since the 1930s- An overview," Sensors International, vol. 3, Jan. 2022, Art. no. 100182.

[6] S. Raha, Md. Ahmaruzzaman, "ZnO nanostructured materials and their potential applications: progress, challenges and perspectives," Nanoscale Advances, vol. 4, no. 8, pp. 1868–1925, 2022.

[7] G. Dutta, A. Sugumaran, "Bioengineered zinc oxide nanoparticles: Chemical, green, biological fabrication methods and its potential biomedical applications," Journal of Drug Delivery Science and Technology, vol. 66, Dec. 2021, Art. no. 102853.

[8] K. Bachhav, A. S. Garde, "Versatile synthesis of zinc oxide nanoparticles via chemical route: A review," Materials Today: Proceedings, Aug. 2023.

[9] D.-M. Radulescu, V.-A. Surdu, A. Ficai, D. Ficai, A.-M. Grumezescu, E. Andronescu, "Green synthesis of metal and metal oxide nanoparticles: A review of the principles and biomedical applications," International Journal of Molecular Sciences, vol. 24, no. 20, 2023, Art. no. 15397.

[10] J. Singh, T. Dutta, K.-H. Kim, M. Rawat, P. Samddar, P. Kumar, "'Green' synthesis of metals and their oxide nanoparticles: applications for environmental remediation," Journal of Nanobiotechnology, vol. 16, no. 1, 2018, Art. no. 84.

[11] H. Al Jabri, M. H. Saleem, M. Rizwan, I. Hussain, K. Usman, M. Alsafran, "Zinc Oxide nanoparticles and their biosynthesis: Overview," Life, vol. 12, no. 4, Apr. 2022, Art. no. 594.

[12] J. Xu, Y. Huang, S. Zhu, N. Abbes, X. Jing, L. Zhang, "A review of the green synthesis of ZnO nanoparticles using plant extracts and their prospects for application in antibacterial textiles," Journal of Engineered Fibers and Fabrics, vol. 16, 2021, Art. no. 15589250211046242.

[13] A. Kavitha, A. Doss, R. P. Praveen Pole, T. P. K. Pushpa Rani, R. Prasad, S. Satheesh, "A mini review on plant-mediated zinc oxide nanoparticles and their antibacterial potency," Biocatalysis and Agricultural Biotechnology, vol. 48, Mar. 2023, Art. no. 102654.

[14] A. G. Kaningini, S. Azizi, N. Sintwa, K. Mokalane, K. C. Mohale, F. N. Mudau, M. Maaza, "Effect of optimized precursor concentration, temperature, and doping on optical properties of ZnO nanoparticles synthesized via a green route using bush tea (*Athrixia phylicoides* DC.) leaf extracts," ACS Omega, vol. 7, no. 36, pp. 31658–31666, Sep. 2022.

[15] V. Batra, I. Kaur, D. Pathania, Sonu, V. Chaudhary, "Efficient dye degradation strategies using green synthesized ZnO-based nanoplatforms: A review," Applied Surface Science Advances, vol. 11, Oct. 2022, Art. no. 100314.

[16] G. T. Tran, N. T. H. Nguyen, N. T. T. Nguyen, T. T. T. Nguyen, D. T. C. Nguyen, T. V. Tran, "Formation, properties and applications of microalgae-based ZnO nanoparticles: A review," Journal of Environmental Chemical Engineering, vol. 11, no. 5, Oct. 2023, Art. no. 110939.

[17] M. Naseer, U. Aslam, B. Khalid, B. Chen, "Green route to synthesize zinc oxide nanoparticles using leaf extracts of *Cassia fistula* and *Melia azadarach* and their

antibacterial potential," Scientific Reports, vol. 10, no. 1, 2020, Art. no. 9055.

[18] S. Faisal, H. Jan, S. A. Shah, S. Shah, A. Khan, M. T. Akbar, M. Rizwan, F. Jan, Wajidullah, N. Akhtar, A. Khattak, S. Syed, "Green synthesis of zinc oxide (ZnO) nanoparticles using aqueous fruit extracts of *Myristica fragrans*: Their characterizations and biological and environmental Applications," ACS Omega, vol. 6, no. 14, pp. 9709–9722, Apr. 2021.

[19] B. Naiel, M. Fawzy, M. W. A. Halmy, A. E. D. Mahmoud, "Green synthesis of zinc oxide nanoparticles using Sea Lavender (*Limonium pruinosum* L. Chaz.) extract: characterization, evaluation of anti-skin cancer, antimicrobial and antioxidant potentials," Scientific Reports, vol. 12, no. 1, 2022, Art. no. 20370.

[20] T. U. Doan Thi, T. T. Nguyen, Y. D. Thi, K. H. Ta Thi, B. T. Phan, K. N. Pham, "Green synthesis of ZnO nanoparticles using orange fruit peel extract for antibacterial activities," RSC Advances, vol. 10, no. 40, pp. 23899–23907, 2020.

[21] J. Ali, S. Bibi, W. B. Jatoi, M. Tuzen, M. A. Jakhrani, X. Feng, T. A. Saleh, "Green synthesized zinc oxide nanostructures and their applications in dye-sensitized solar cells and photocatalysis: A review," Materials Today Communications, vol. 36, Aug. 2023, Art. no. 106840.

[22] R. Álvarez-Chimal, V. I. García-Pérez, M. A. Álvarez-Pérez, R. Tavera-Hernández, L. Reyes-Carmona, M. Martínez-Hernández, J. Á. Arenas-Alatorre, "Influence of the particle size on the antibacterial activity of green synthesized zinc oxide nanoparticles using *Dysphania ambrosioides* extract, supported by molecular docking analysis," Arabian Journal of Chemistry, vol. 15, no. 6, Jun. 2022, Art. no. 103804.

[23] C. Vivek, B. Balraj, S. Thangavel, "Structural, optical and electrical behavior of ZnO@Ag core–shell nanocomposite synthesized via novel plasmon-green mediated approach," Journal of Materials Science: Materials in Electronics, vol. 30, no. 12, pp. 11220–11230, 2019.

[24] H. Mirzaei, M. Darroudi, "Zinc oxide nanoparticles: Biological synthesis and biomedical applications," Ceramics International, vol. 43, no. 1, pp. 907–914, Jan. 2017.

[25] H. Mohd Yusof, N. Abdul Rahman, R. Mohamad, U. H. Zaidan, A. A. Samsudin, "Biosynthesis of zinc oxide nanoparticles by cell-biomass and supernatant of *Lactobacillus plantarum* TA4 and its antibacterial and biocompatibility properties," Scientific Reports, vol. 10, no. 1, 2020, Art. no. 19996.

[26] S. W. Balogun, O. O. James, Y. K. Sanusi, O. H. Olayinka, "Green synthesis and characterization of zinc oxide nanoparticles using bashful (*Mimosa pudica*), leaf extract: a precursor for organic electronics applications," SN Applied Sciences, vol. 2, no. 3, 2020., Art. no. 504.

[27] A. S. Abdelbaky, A. M. H. A. Mohamed, M. Sharaky, N. A. Mohamed, Y. M. Diab, "Green approach for the synthesis of ZnO nanoparticles using *Cymbopogon citratus* aqueous leaf extract: characterization and evaluation of their biological activities," Chemical and Biological Technologies in Agriculture, vol. 10, no. 1, 2023, Art. no. p. 63.

[28] A. Yıldırım, A. Mavi, A. A. Kara, "Antioxidant and antimicrobial activities of *Polygonum cognatum* Meissn extracts," Journal of the Science of Food and Agriculture, vol. 83, no. 1, pp. 64–69, Jan. 2003.

[29] F. Demirgül, M. Divriklioğlu-Kundak, O. Sağdıç, "Bioactive properties, antibacterial activity, and color features of *Polygonum cognatum*: The effects of frozen storage and cooking process," Food Science and

Technology, vol. 42, Jul. 2022, Art. no. e00322.

[30] Ö. Ergen Akçin, Y. Akçin, M. K. Akbulut, "The ethnobotanical and anatomical properties of *Polygonum cognatum* Meıssn. (Polygonaceae)," Biological Diversity and Conservation, vol. 7, no. 2, pp. 117–121, 2014.

[31] H. Saraç, T. Daştan, A. Demirbaş, S. Durna Daştan, T. Karaköy, H. Durukan, "Nutrient composition and in vitro anti-carcinogenic activity of knotweed (*Polygonum cognatum* Meissn.) plant extracts," (in Turkish), Ziraat Fakültesi Dergisi, pp. 340–347, 2018.

[32] H. İ. Ulusoy, H. Acıdereli, U. Tutar, "Optimization of extraction parameters for fat soluble vitamins and major element analysis in Polygonum cognatum Meıssn plant (Madımak)," Journal of the Turkish Chemical Society Section A: Chemistry, vol. 4, no. 1, pp. 165–178, 2017.

[33] A. Gümüşçü, S. Dinç, M. Kara, M. Akkuş, G. Gümüşçü, "Phenolic compounds of natural knotweed (*Polygonum cognatum* Meissn.) populations from Turkey," International Journal of Plant Based Pharmaceuticals, vol. 2, no. 1, pp. 37–41, 2022.

[34] S. Ulusoy, S. Erdoğan, M. G. Karaaslan, B. Ateş, H. İ. Ulusoy, S. Erdemoğlu, "Optimization of extraction parameters for folic acid and antioxidant compounds from an edible plant (*Polygonum Cognatum* Meissn) using pressurized liquid extraction (PLE) system," Cumhuriyet Science Journal, vol. 39, no. 4, pp. 1069–1080, 2018.

[35] R. Akpınar, G. Yıldırım Baştemur, B. Bıçak, N. O. Sanli, E. Mertoğlu Kamalı, M. Pekmez, S. Kecel Gündüz, S. Perçin Özkorucuklu, "Phytochemical profiling, in vitro biological activities, and in silico (molecular docking and absorption, distribution, metabolism, excretion, toxicity) studies of *Polygonum cognatum* Meissn," Journal of Separation Science, vol. 47, no. 1, 2024, Art. no. 2300750.

[36] S. Pekdemir, M. Çiftci, M. Karatepe, "Determination of in vitro biological activities and some phytochemical components of *Polygonum cognatum* Meissn (Madımak) plant grown in Elazığ," (in Turkish), Avrupa Bilim ve Teknoloji Dergisi, no. 18, pp. 368–378, 2020.

[37] M. Bayram, S. Topuz, "Optimization of phenolic compound extraction using response surface method from Madımak (*Polygonum cognatum* Meissn.)," (in Turkish), Gıda, vol. 48, no. 1, pp. 118–129, 2023.

[38] N. Eruygur, E. Ucar, M. Ataş, M. Ergul, M. Ergul, F. Sozmen, "Determination of biological activity of *Tragopogon porrifolius* and *Polygonum cognatum* consumed intensively by people in Sivas," Toxicology Reports, vol. 7, pp. 59–66, Jan. 2020.

[39] Ö. Çevik, A. Şener, Z. Özdemir Kumral, Ş. Çetinel, A. Altıntaş, R. Oba, B. Yeğen, A. Yarat, "Protective and therapeutic effects of *Polygonum cognatum* Meissn aqueous extract in experimental colitis," Marmara Pharmaceutical Journal, vol. 18, no. 3, pp. 126–134, 2014.

[40] S. Gözcü, R. A. Uğan, H. Özbek, B. Gündoğdu, Z. Güvenalp, "Evaluation of antidiabetic and antioxidant effects of *Polygonum cognatum* Meisn. and phytochemical analysis of effective extracts," Biomedical Chromatography, vol. 38, no. 3, 2024, Art. no. e5809.

[41] N. Gürsoy, S. Elagöz, E. Gölge, "Investigation of antimicrobial effects of silver nanoparticles (AgNPs) synthesized on Polygonum cognatum Meissn. and fungus environment," (in Turkish), Türk Tarım ve Doğa Bilimleri Dergisi, vol. 7, no. 1, pp. 221–230, 2020.

[42] M. Yilmaz, A. Yilmaz, A. Karaman, F. Aysin, O. Aksakal, "Monitoring

chemically and green-synthesized silver nanoparticles in maize seedlings via surface-enhanced Raman spectroscopy (SERS) and their phytotoxicity evaluation," Talanta, vol. 225, 2021, Art. no. 121952.

[43] Ö. Kaplan, N. Gökşen Tosun, "Biosynthesis of iron, copper and silver nanoparticles using *Polygonum Cognatum* and *Tragopogon Porrifolius* extracts and evaluation of their antimicrobial potentials," Düzce University Journal of Science and Technology, vol. 11, no. 4, pp. 2155–2167, 2023.

[44] H. Meskher, S. B. Belhaouari, K. Deshmukh, C. M. Hussain, F. Sharifianjazi, "A magnetite composite of molecularly imprinted polymer and reduced graphene oxide for sensitive and selective electrochemical detection of catechol in water and milk samples: an artificial neural network (ANN) application," Journal of The Electrochemical Society, vol. 170, no. 4, Apr. 2023, Art. no. 047502.

[45] L. Lutterotti, "Total pattern fitting for the combined size–strain–stress–texture determination in thin film diffraction," Nuclear Instruments and Methods in Physics Research Section B: Beam Interactions with Materials and Atoms, vol. 268, no. 3, pp. 334–340, 2010.

[46] V. D. Mote, Y. Purushotham, B. N. Dole, "Williamson-Hall analysis in estimation of lattice strain in nanometer-sized ZnO particles," Journal of Theoretical and Applied Physics, vol. 6, no. 1, 2012, Art. no. 6.

[47] S. Gražulis, D. Chateigner, R. T. Downs, A. F. T. Yokochi, M. Quirós, L. Lutterotti, E. Manakova, J. Butkus, P. Moeck, A. Le Bail, "Crystallography Open Database – an open-access collection of crystal structures," Journal of Applied Crystallography, vol. 42, no. 4, pp. 726–729, Aug. 2009.

[48] S. Mansy, H. Musleh, S. Shaat, J. Asad, N. AlDahoudi, "Computational and experimental study of wurtzite phase ZnO nanoparticles," Materials Today Communications, vol. 35, 2023, Art. no. 105688.

[49] J. Vera, W. Herrera, E. Hermosilla, M. Díaz, J. Parada, A. B. Seabra, G. Tortella, H. Pesenti, G. Ciudad, O. Rubilar, "Antioxidant activity as an indicator of the efficiency of plant extract-mediated synthesis of zinc oxide nanoparticles," Antioxidants, vol. 12, no. 4, 2023, Art. no. 784.

[50] Q. P. Pham, Q. N. Le Nguyen, N. H. Nguyen, U. T. T. Doan, T. D. T. Ung, V. C. Tran, T. B. Phan, A. T. T. Pham, N. K. Pham, "Calcination-dependent microstructural and optical characteristics of eco-friendly synthesized ZnO nanoparticles and their implementation in analog memristor application," Ceramics International, vol. 49, no. 12, pp. 20742–20755, 2023.

[51] H. Naseer, T. Iqbal, "Green synthesis of silver-doped zinc oxide nanoparticles for investigation of their photocatalytic activity and shelf life applications," Biomass Conversion and Biorefinery, 2023.

[52] K. Dulta, G. Koşarsoy Ağçeli, P. Chauhan, R. Jasrotia, P. K. Chauhan, "A novel approach of synthesis zinc oxide nanoparticles by *Bergenia ciliata* Rhizome extract: Antibacterial and anticancer potential," Journal of Inorganic and Organometallic Polymers and Materials, vol. 31, no. 1, pp. 180–190, 2021.

[53] M. Jarvin, S. A. Kumar, D. R. Rosaline, E. L. Foletto, G. L. Dotto, S. S. R. Inbanathan, "Remarkable sunlight-driven photocatalytic performance of Ag-doped ZnO nanoparticles prepared by green synthesis for degradation of emerging pollutants in water," Environmental Science and Pollution Research, vol. 29, no. 38, pp. 57330–57344, 2022.

[54] A. Jayachandran, A. T.R., A. S. Nair, "Green synthesis and characterization of zinc oxide nanoparticles using *Cayratia pedata* leaf extract," Biochemistry and Biophysics Reports, vol. 26, 2021, Art. no. 100995.

[55] A. Sangeetha, S. Jaya Seeli, K. P. Bhuvana, M. A. Kader, S. K. Nayak, "Correlation between calcination temperature and optical parameter of zinc oxide (ZnO) nanoparticles," Journal of Sol-Gel Science and Technology, vol. 91, no. 2, pp. 261–272, 2019.

[56] R. Cuscó, E. Alarcón-Lladó, J. Ibáñez, L. Artús, J. Jiménez, B. Wang, M. J. Callahan, "Temperature dependence of Raman scattering in ZnO," Physical Review B, vol. 75, no. 16, Apr. 2007, Art. no. 165202.

[57] S. Knust, L. Ruhm, A. Kuhlmann, D. Meinderink, J. Bürger, J. K. N. Lindner, M. T. de los Arcos de Pedro, G. Grundmeier, "In situ backside Raman spectroscopy of zinc oxide nanorods in an atmospheric-pressure dielectric barrier discharge plasma," Journal of Raman Spectroscopy, vol. 52, no. 7, pp. 1237–1245, Jul. 2021.

[58] A. K. Rana, Y. Kumar, P. Rajput, S. N. Jha, D. Bhattacharyya, P. M. Shirage, "Search for origin of room temperature ferromagnetism properties in Ni-doped ZnO nanostructure," ACS Applied Materials & Interfaces, vol. 9, no. 8, pp. 7691–7700, Mar. 2017.

[59] D. Kumar, M. K. Singh, M. S. Mehata, "Exploration of grown cobalt-doped zinc oxide nanoparticles and photodegradation of industrial dye," Materials Research Bulletin, vol. 150, Jun. 2022, Art. no. 111795.

[60] R. D. Chandra, L. Veena, K. G. Gopchandran, "Suppression of visible emission in low-temperature synthesized cobalt-doped ZnO nanoparticles and their photosensing applications," Inorganic Chemistry, vol. 62, no. 29, pp. 11360–11371, Jul. 2023.

[61] F. J. Manjón, B. Marí, J. Serrano, A. H. Romero, "Silent Raman modes in zinc oxide and related nitrides," Journal of Applied Physics, vol. 97, no. 5, Feb. 2005, Art. no. 053516.

[62] P. Makuła, M. Pacia, W. Macyk, "How to correctly determine the band gap energy of modified semiconductor photocatalysts based on UV–Vis spectra," The Journal of Physical Chemistry Letters, vol. 9, no. 23, pp. 6814–6817, Dec. 2018.

[63] N. Rana, S. Chand, A. K. Gathania, "Green synthesis of zinc oxide nano-sized spherical particles using *Terminalia chebula* fruits extract for their photocatalytic applications," International Nano Letters, vol. 6, no. 2, pp. 91–98, 2016.

[64] G. Tang, S. Tian, Z. Zhou, Y. Wen, A. Pang, Y. Zhang, D. Zeng, H. Li, B. Shan, C. Xie, "ZnO micro/nanocrystals with tunable exposed (0001) facets for enhanced catalytic activity on the thermal decomposition of ammonium perchlorate," The Journal of Physical Chemistry C, vol. 118, no. 22, pp. 11833–11841, Jun. 2014.

[65] X. Meng, L. Jiang, W. Wang, Z. Zhang, "Enhanced photocatalytic activity of BiOBr/ZnO heterojunction semiconductors prepared by facile hydrothermal method," International Journal of Photoenergy, vol. 2015, 2015, Art. no. 747024.

[66] K. X. Yao, R. Sinclair, H. C. Zeng, "Symmetric linear assembly of hourglass-like ZnO nanostructures," The Journal of Physical Chemistry C, vol. 111, no. 5, pp. 2032–2039, Feb. 2007.

[67] J. M. Hancock, W. M. Rankin, B. Woolsey, R. S. Turley, R. G. Harrison, "Controlled formation of ZnO hexagonal prisms using ethanolamines and water," Journal of Sol-

Gel Science and Technology, vol. 84, no. 1, pp. 214–221, 2017.

[68] D. Li, J. Wang, X. Wu, C. Feng, X. Li, "Ultraviolet-assisted synthesis of hourglass-like ZnO microstructure through an ultrasonic and microwave combined technology," Ultrasonics Sonochemistry, vol. 20, no. 1, pp. 133–136, 2013.

[69] M. Turan, S. Kordali, H. Zengin, A. Dursun, Y. Sezen, "Macro and micro mineral content of some wild edible leaves consumed in Eastern Anatolia," Acta Agriculturae Scandinavica, Section B — Soil & Plant Science, vol. 53, no. 3, pp. 129–137, Jan. 2003.